Electronic Supplementary Material (ESI) for Nanoscale Horizons.

Supporting Information

A new approach for ultrasensitive tactile sensor covering ultrawide pressure range based on hierarchical pressure-peak effect

Congyi Wu [a,b], Tian Zhang [a], Jian Zhang [a], Jin Huang [d*], Xing Tang [a], Tingting Zhou [a], Youmin Rong [b], Yu Huang [b], Songxin Shi [b], Dawen Zeng [a,c*]

[a] State Key Laboratory of Materials Processing and Die Mould Technology, Huazhong University of Science and Technology (HUST), Wuhan 430074, China

[b] State Key Laboratory of Digital Manufacturing Equipment and Technology, Huazhong University of Science and Technology (HUST), Wuhan 430074, China

[c] Hubei Collaborative Innovation Center for Advanced Organic Chemical Materials, Hubei University, Wuhan 430074, China.

[d] Chongqing Key Laboratory of Soft-Matter Material Chemistry and Function Manufacturing, School of Chemistry and Chemical Engineering, Southwest University, Chongqing 400715, China.

Contents:

1. Supplementary instructions for the HPPE tactile sensor manufacturing process

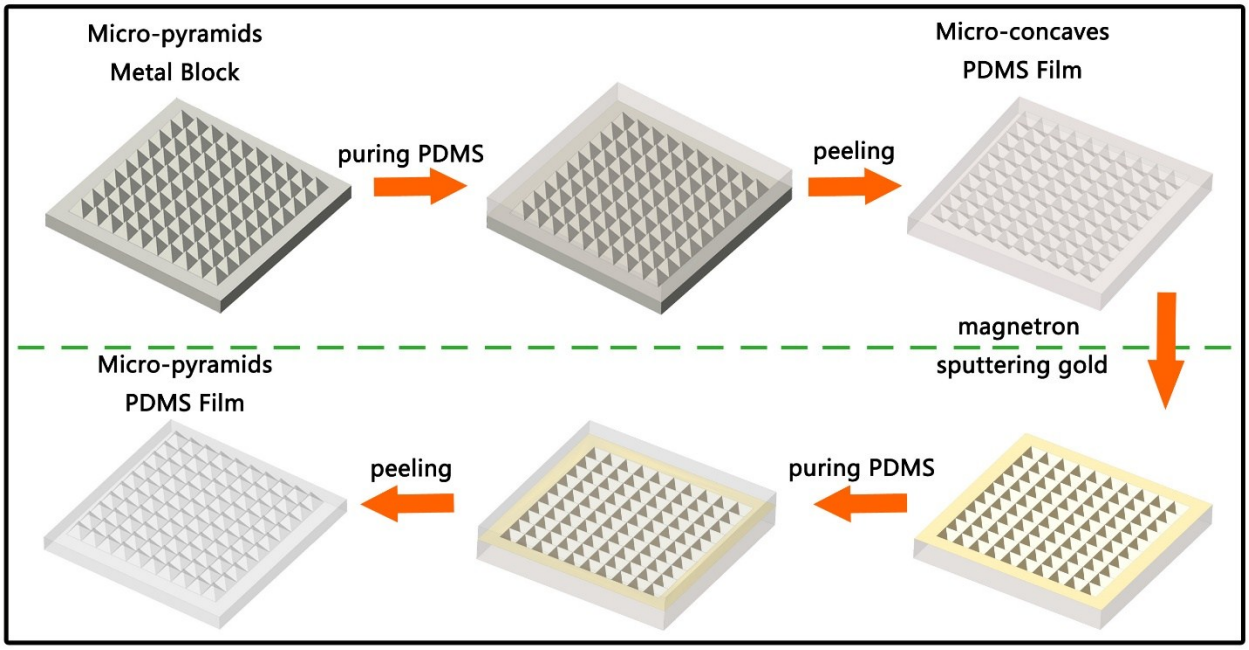

Figure S1. Preparation of the micro-pyramids PDMS film via two-steps soft lithography replication process.

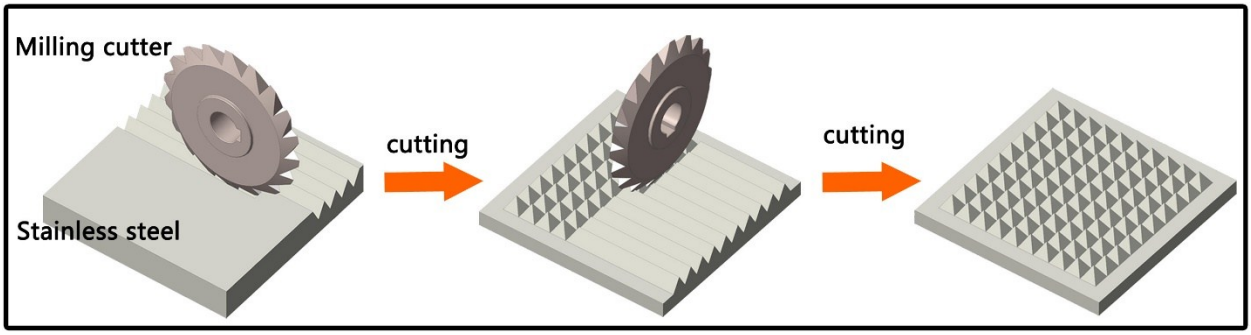

Figure S2. Schematic illustration of fabricating the micro-pyramid metal template.

2. Optical characteristics of the HPPE tactile sensor

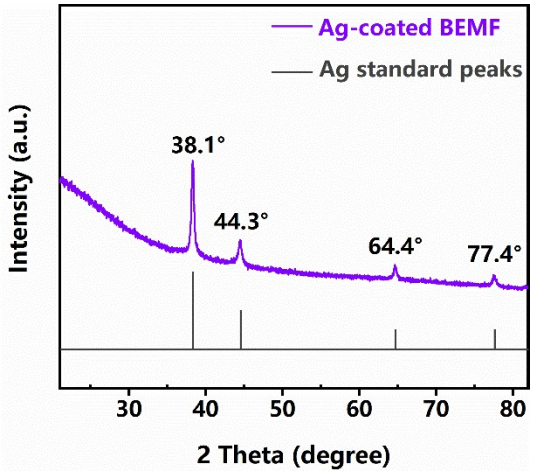

Figure S3. X-ray diffraction (XRD) pattern of the ELD-Ag PDMS film. The peaks at four different 2theta positions of 38.1°, 44.3°, 64.4°and 77.4° are corresponded to (1 1 1), (2 0 0), (2 2 0) and (3 1 1) crystal planes of silver respectively. These peaks confirm that the silver particles successfully deposit on the surface of the micro-pyramids PDMS film.

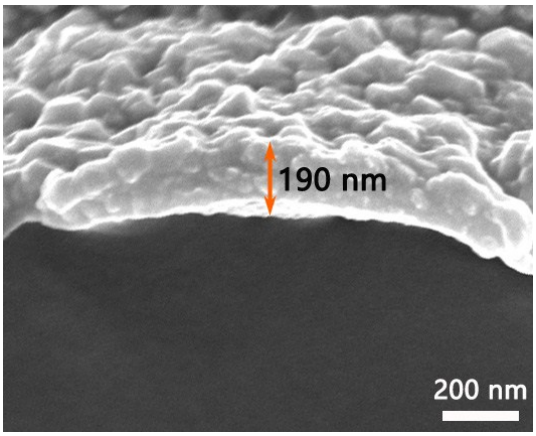

Figure S4. Cross-sectional scanning electron microscopy (SEM) image of the ELD-Ag PDMS film and the silver layer is 190 nm thick.

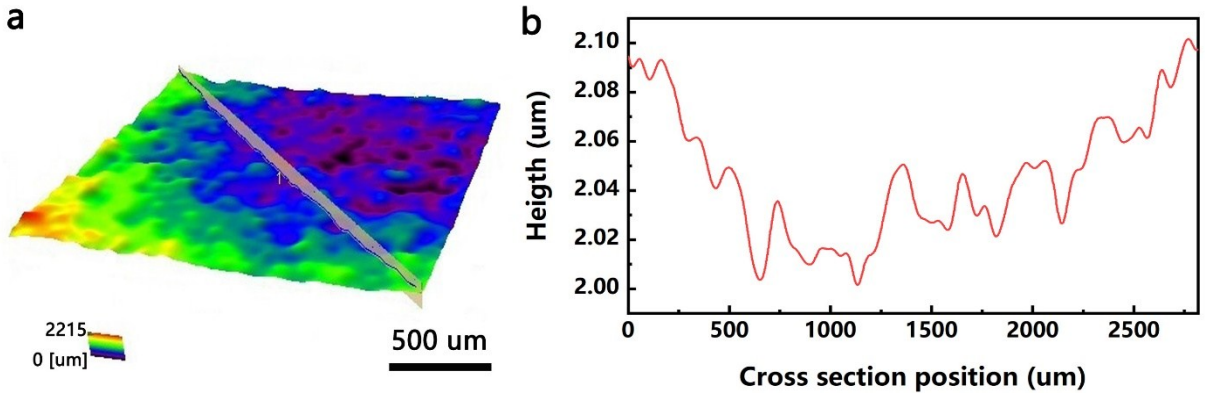

Figure S5. 3D features of the ELD-Ag PDMS film.

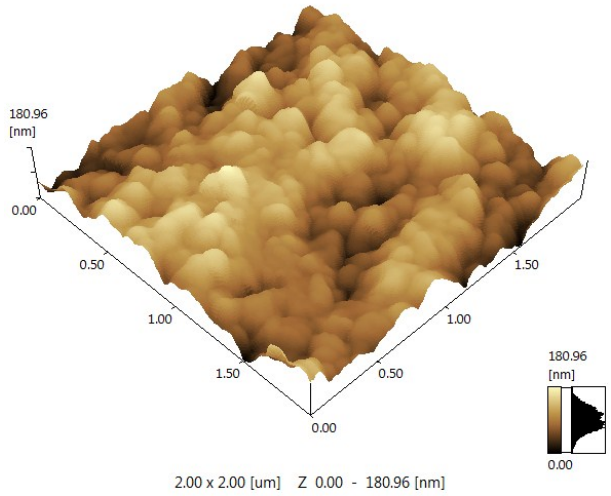

Figure S6. Atomic Force Microscope (AFM) images of the ELD-Ag PDMS film. It shows that the silver grows uniformly on the PDMS film with the grain size below 200 nm.

3. Performance comparison of the proposed tactile sensor

Table S1. Key parameters of the HPPE tactile sensor and recently developed piezoresistive flexible pressure sensors.

Active Materials	Sensitivity (kPa^{-1})	Pressure range (kPa)	Ref.
ELD-Ag	*11.6, 1608.75 and 43.95*	*0.04-4, 4-450 and 450-700*	*Our work*
Gold nanowires	1.14	< 5	[41]
Silver nanowires	3.8, 0.8 and 0.35	< 0.5, 0.5-2.5 and 2.5-4.5	[42]
Copper nanowires	0.16	0.03-0.21	[43]
rGO	5.53 and 0.01	< 0.1and 0.1-1.4	[27]
GO	0.96 and 0.005	< 49.5 and 49.5-113	[39]
rGO	2.5, 12; 951 and 470	0.01-1, 1-50, 50-200 and 200-400	[31]
GO/PVA	4.52 and 28.34	< 3 and 3-10	[30]
Au/PPY	1.8 and 0.03	0.002-0.35 and 0.35-3	[29]
rGO/PVDF	3.1 and 15.6	< 0.06 and 0.06-55	[10]
rGO/PVDF	47.7	0.0013-353	[36]

41. S. Gong, W. Schwalb, Y. Wang, Y. Chen, Y. Tang, J. Si, B. Shirinzadeh and W. Cheng, Nature Communications, 2014, **5**.

42. Y. Joo, J. Byun, N. Seong, J. Ha, H. Kim, S. Kim, T. Kim, H. Im, D. Kim and Y. Hong, Nanoscale, 2015, **7**, 6208-6215.

43. X. Xu, R. Wang, P. Nie, Y. Cheng, X. Lu, L. Shi and J. Sun, ACS applied materials & interfaces, 2017, **9**, 14273-14280.

27. B. Zhu, Z. Niu, H. Wang, W. R. Leow, H. Wang, Y. Li, L. Zheng, J. Wei, F. Huo and X. J. S. Chen, Small, 2014, **10**, 3625-3631.

39. H. Tian, Y. Shu, X.-F. Wang, M. A. Mohammad, Z. Bie, Q.-Y. Xie, C. Li, W.-T. Mi, Y. Yang and T.-L. J. S. r. Ren, Scientific Reports, 2015, **5**, 8603.

31. X. Tang, C. Wu, L. Gan, T. Zhang, T. Zhou, J. Huang, H. Wang, C. Xie and D. J. S. Zeng, Small, 2019, **15**, 1804559.

30. W. Liu, N. Liu, Y. Yue, J. Rao, F. Cheng, J. Su, Z. Liu and Y. J. S. Gao, Small, 2018, **14**, 1704149.

29. Q. Shao, Z. Niu, M. Hirtz, L. Jiang, Y. Liu, Z. Wang and X. J. S. Chen, Small, 2014, **10**, 1466-1472.

10. Z. Lou, S. Chen, L. Wang, K. Jiang and G. J. N. E. Shen, Nano Energy, 2016, **23**, 7-14.

36. Y. Lee, J. Park, S. Cho, Y.-E. Shin, H. Lee, J. Kim, J. Myoung, S. Cho, S. Kang and C. J. A. n. Baig, ACS Nano, 2018, **12**, 4045-4054.

4. Sensing performances supplement of the HPPE tactile sensor

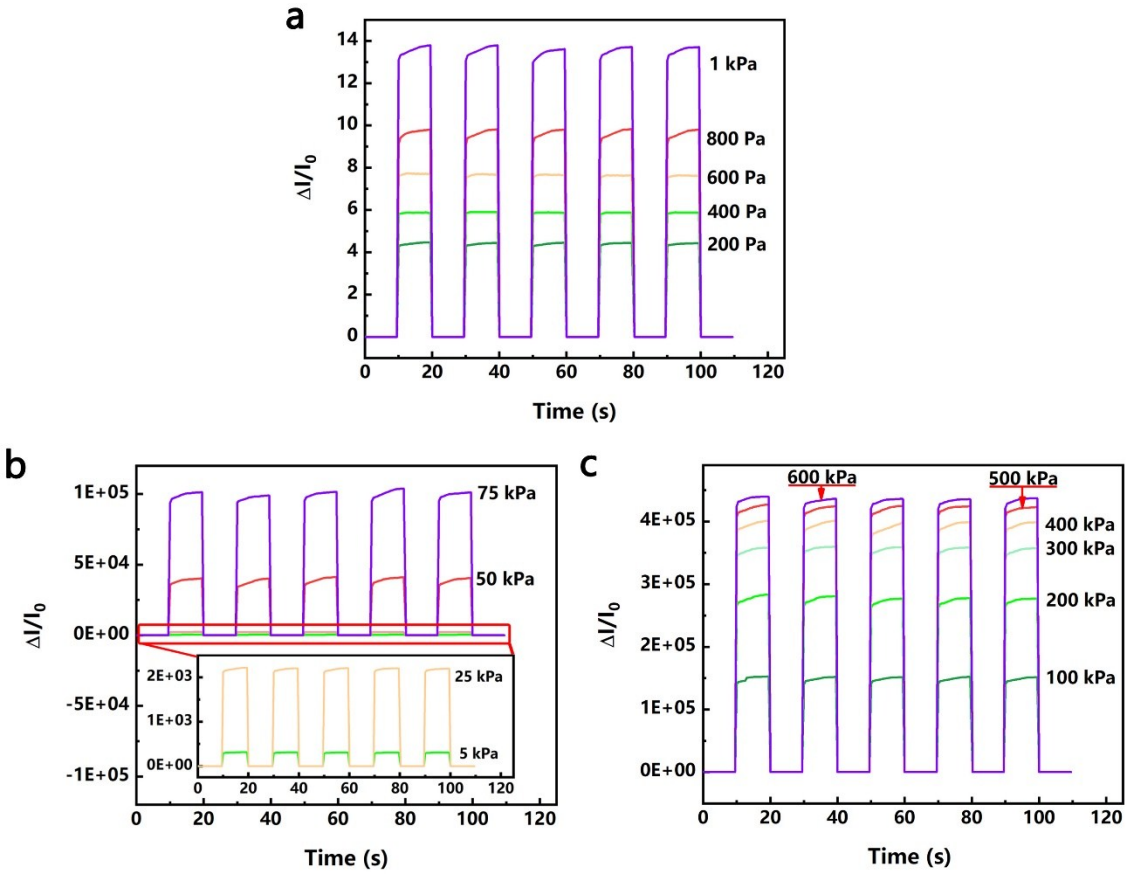

Figure S7. a-c) The transient response of loading and unloading when the same pressure is applied repeatedly for five cycles, corresponding pressures from 0.2 to 600 kPa, respectively.

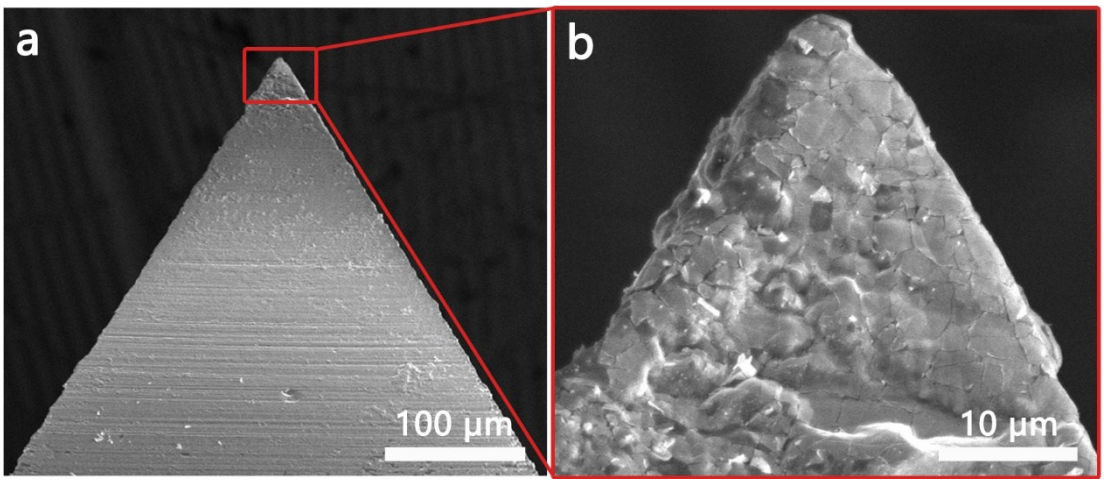

Figure S8. a) Low - and a) High -magnification SEM images of the ELD-Ag PDMS micro-pyramid after the 10,000 compression deformation tests. Micro-cracks appeared on the surface of the silver layer due to the modulus mismatch. At the same time, the micro-cracks do not shed significantly due to the strong adhesion of the silver.

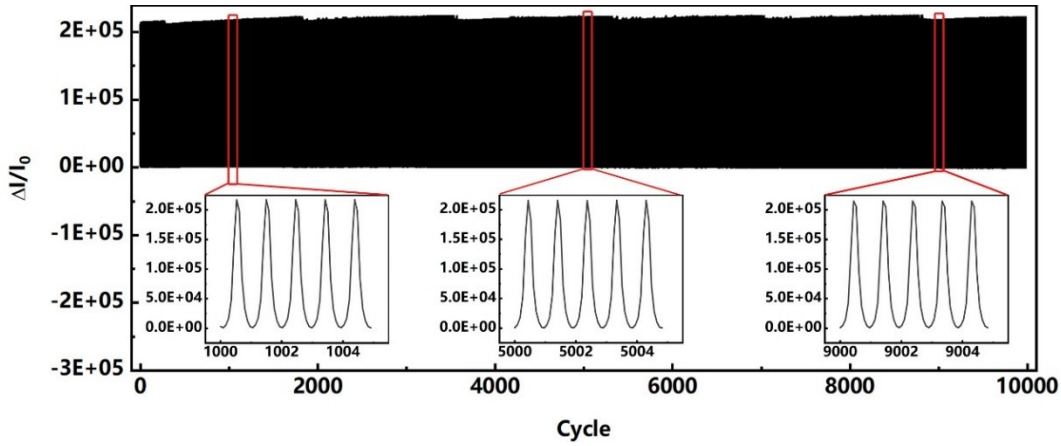

Figure S9. Fatigue tests of the HPPE tactile sensor under 100 kPa with more than 10000 cycles when magnetron sputtering Au/PET electrode instead of PET/ITO electrode.

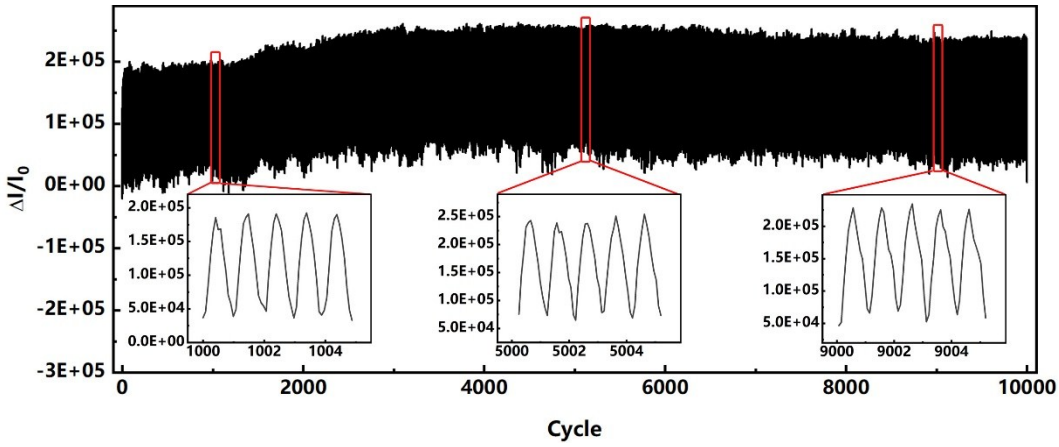

Figure S10. Fatigue tests of the HPPE tactile sensor under 100 kPa with more than 10000 cycles when magnetron sputtering Ag process instead of ELD-Ag process.

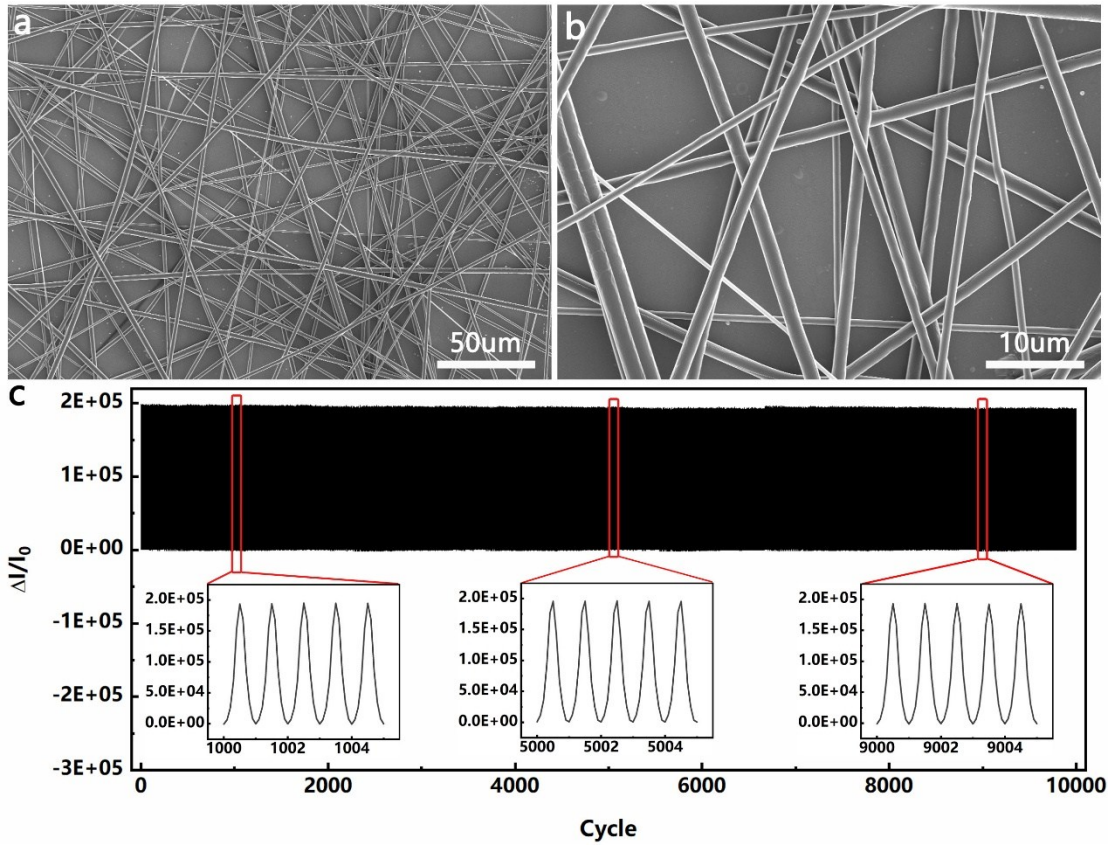

Figure S11. a) Low- and b) High-magnification SEM images of the insulating PVANW networks. c) Fatigue tests of the HPPE tactile sensor under 100 kPa with more than 10000 cycles when magnetron sputtering Ag process instead of ELD-Ag process.

5. Calculation S1: The pyramid surface resistance (R_s)

The conductivity ρ of the magnetron sputtered silver layer with a thickness t of 50 nm was 5.3 $\times 10^7$ S/m measured by a four-probe method. When the pyramid height is 0.3 mm and the included angle θ between pyramid surface and bottom surface is 60° (As shown in **figure 1c**, assume the rounded corners of the pyramid top are 2 um), calculate the surface resistance of a single pyramid:

$$R=\int_{0.0002}^{0.3}\frac{\rho\tan\theta}{8tx}dx \tag{S1}$$

Therefore, when the pyramid is unpressurized, R_s has a maximum value of 0.15 Ω, and the resistance value of the pyramid gradually decreases after being compressed. Compared to the top contact resistance of the pyramid (R_c), R_s of the pyramid has little effect on the change of the overall resistance of the single pyramid.

6. Experimental setup

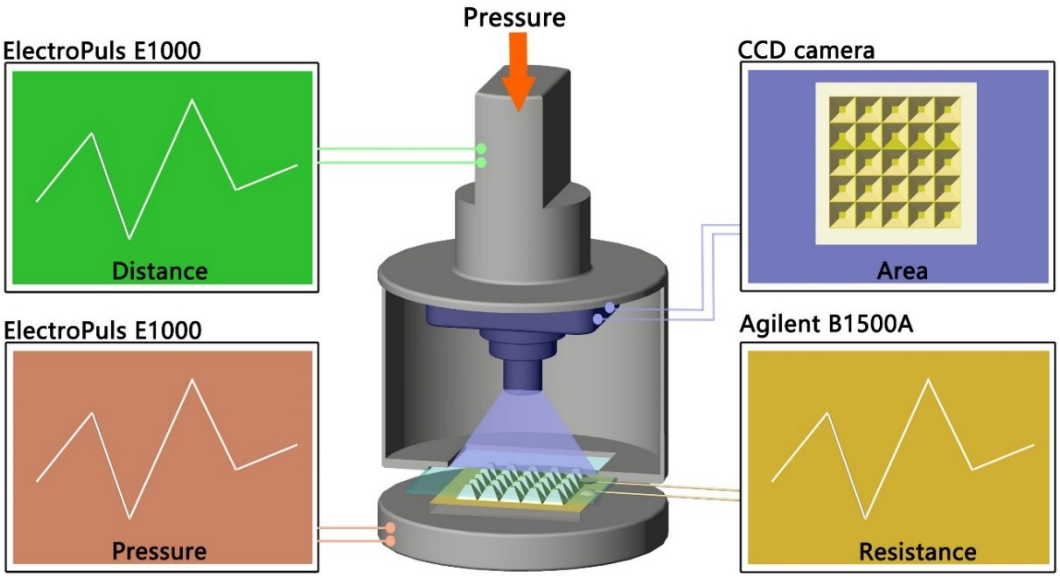

Figure S12. Detailed schematic of the experimental setup. In order to explore the PPE of piezoresistive pressure sensor, distance, pressure, contact area and resistance are measured simultaneously during compression deformation.

7. Quantitative analysis of contact area change in PPE

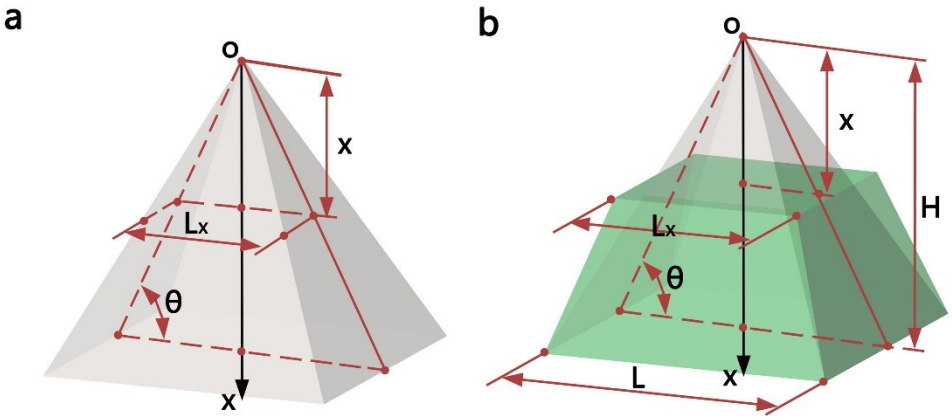

Figure S13. Schematic for calculating pyramid contact area base on a) the cross-sectional area and b) the same volume principle.

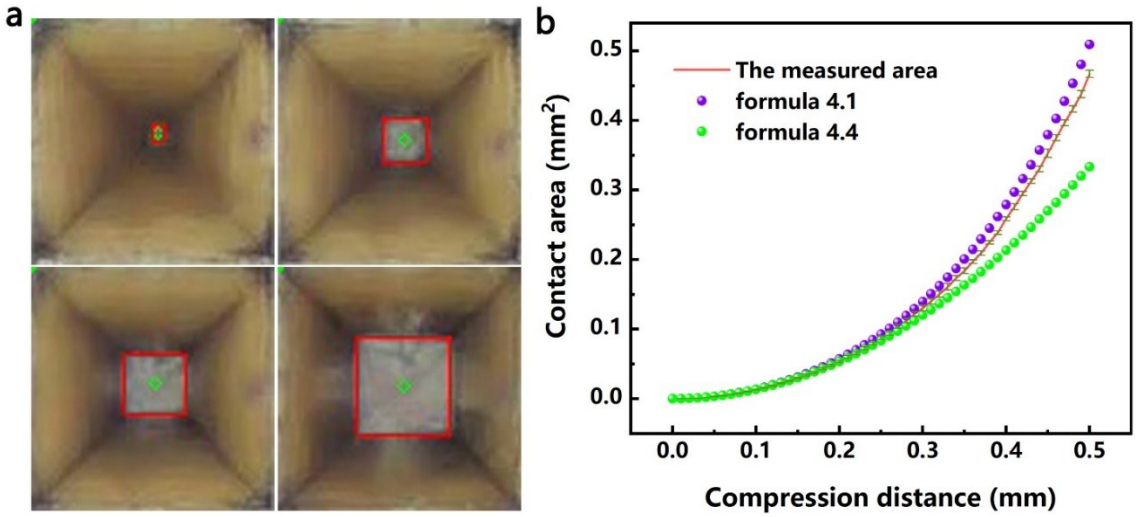

Figure S14. a) CCD images of individual pyramids at different compression displacements. b) The comparison between the actual contact area and the calculated contact area.

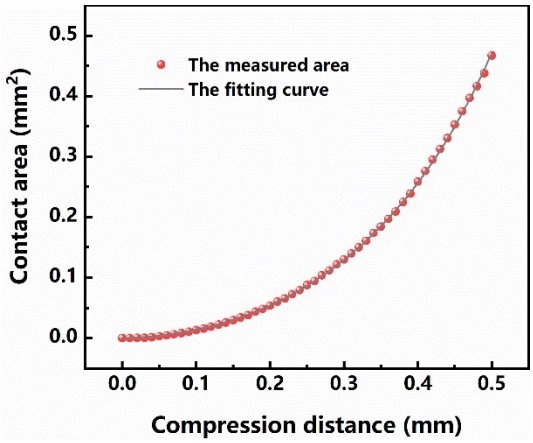

Figure S15 Curve fitting of pyramid contact area based on equation S6.

8. Calculation S2: The contact resistance (R_c)

The change of contact area can be quantitatively described by mathematical equation. For a single pyramid, when the deformation of the pyramid itself is not considered, the cross-sectional area of the pyramid is the contact area (Fig. S8a)，and then:

$$L_x = \frac{2x}{\tan\theta}$$

$$S = L_x^2 = \frac{2x}{(\tan\theta)^2} \tag{S2}$$

Where L_x is the side length of the cross section when the compression distance is x, S is the contact area and θ is the angle between the bottom of the pyramid and the slope. When considering the deformation of the pyramid itself, as shown in Fig. S8b, it can be calculated from the law of volume constancy of super-elastomer as follows:

$$\begin{cases} V_1 = V_2 \\ V_1 = \frac{1}{3}L^2 H \\ V_2 = \left(L^2 + L_x^2 + \sqrt{L^2 \times L_x^{\,2}}\right)\frac{H-x}{3} \end{cases} \tag{S3}$$

Solving the equation system S3, we can get a mono basic quadratic equation:

$$(H\text{-}x)L_x^{\,2} + (H\text{-}x)LL_x - xL^2 = 0 \tag{S4}$$

Solving the mono basic quadratic equation S4, and delete the negative solution, we can get:

$$S = \left[\frac{H}{\tan\theta}\left(\sqrt{\frac{H+3x}{H\text{-}x}} - 1\right)\right]^2 \tag{S5}$$

Where V_1, V_2 are the volumes before and after the deformation, H is the height of the pyramid, and L is the side length of the square at the bottom of the pyramid.

Figure S9a shows the CCD image of a single pyramid at different compression displacements. The area enclosed by the red box is the contact area, and the change in contact area of the pyramid during the compression process is calculated by the gray scale change of the pixel points in the red box. After calculating the grayscale pixel point area of 13 samples, the compression distance-contact area curve obtained is shown in **Figure S9b**. Furthermore, by comparing the difference between different calculation methods and the actual contact area, a more accurate calculation

method of contact area is selected. As shown in the **Figure S9**, when the compression distance is small, both equations can simulate the change of contact area well. As the compression distance increases, equation (S5) can better simulate the change of contact area. Here, equation S5 is chosen to quantitatively calculate the relationship between displacement and compression distance. Since the surface deformation of the pyramid surface during compression deformation is not considered, the contact area calculated by equation S5 is larger than the actual contact area. Here, quadratic polynomial is adopted to modify the equation S5, where the constants in the polynomial are the shape factor related to pyramid shape. The revised equation is as follows:

$$S = \left[\frac{\mathrm{H}}{\tan\theta} \left(\sqrt{\frac{H+3x}{\mathrm{H\text{-}x}}} - 1 \right) \right]^2 - 0.203x^2 + 0.026x \tag{S6}$$

As shown in **Figure S10**, the fitting degree between the modified equation S6 and the actual compression distance-contact area curve is more than 99.9%.

9. Quantitative analysis of the PPE

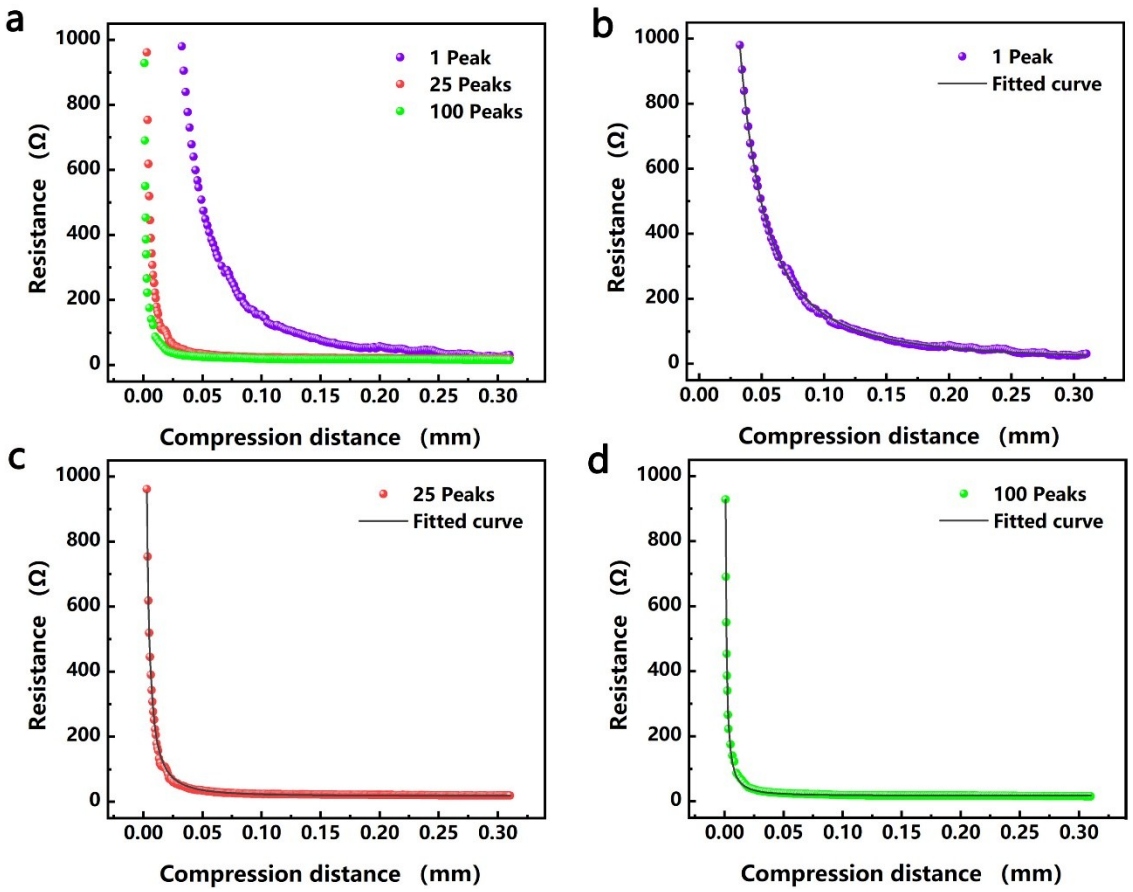

Figure S16. a) Displacements-resistance curves of sensors with different number of pyramids when the silver film thickness of magnetron sputtering is 50 nm. b-d) Each displacement-resistance curve was fitted according to the equation S6.

Table S2. Comparison of the parameters of the distance-resistance curves when the number of pyramids is different according to equation A.

Samples	A	B	R-square
25 nm	0.84868 ± 0.00297	12.28101 ± 0.59949	0.9889
50 nm	0.29517 ± 6.54412E-4	9.96486 ± 0.27701	0.9812
100 nm	0.0759 ± 1.80961E-4	18.1824 ± 0.19528	0.9875

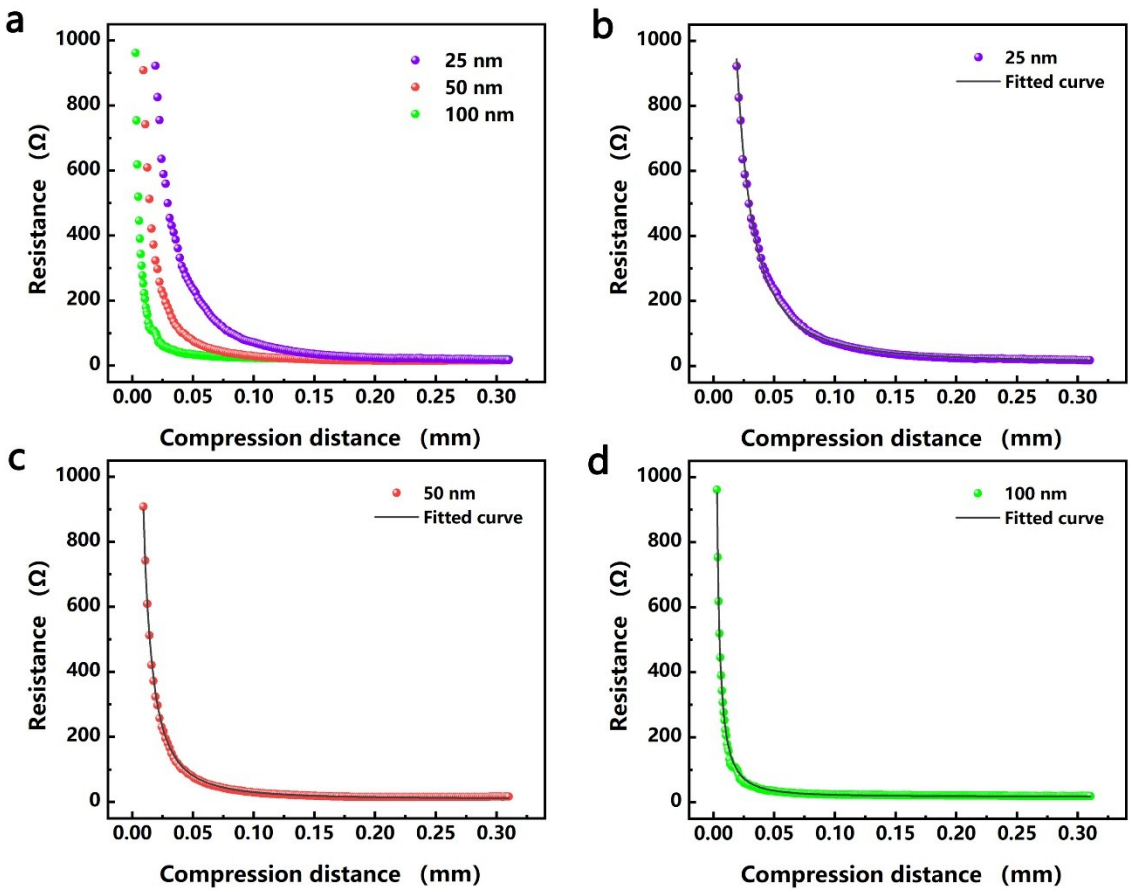

Figure S17. a) Displacements-resistance curves of sensors with different magnetron sputtering silver film thickness the number of pyramids is 25. b-d) Each displacement-resistance curve was fitted according to the equation 4.8.

Table S3. Comparison of the parameters of the distance-resistance curves when the thickness of magnetron sputtering silver is different according to equation A.

Samples	A	B	R-square
1 Peak	1.96934 ± 0.00389	13.60412 ± 0.43553	0.9836
25 Peaks	0.0759 ± 1.80961E-4	18.1824 ± 0.19528	0.9875
100 Peaks	0.02211 ± 6.53753E-5	18.34898 ± 0.31385	0.9834

10. Description of the Movies

Movie S1: The film shows that the HPPE tactile sensor is mounted on the clamp of the Leonardo Da Vinci surgical robot to sense changes in grasping force. According to the change of the sensor signal, the degree of the clamping force is judged to assist the doctor in performing the operation.